Journal of Inflammation Research

Dovepress
Taylor & Francis Group

Open Access Full Text Article

ORIGINAL RESEARCH

Machine Learning-Based Prediction of Post-Operative Systemic Inflammatory Response Syndrome Following Pediatric Percutaneous Nephrolithotripsy

Nueraili Abudurexiti, Bide Liu, Shuheng Wang, Qiang Dong, Maimaitiaili Batuer, Zewei Liu, Xun Li

Department of Urology, People's Hospital of Xinjiang Uygur Autonomous Region, Urumqi, 830001, People's Republic of China

Correspondence: Xun Li, Department of Urology, People's Hospital of Xinjiang Uygur Autonomous Region, No. 91, Tian-Chi Road, Tianshan District, Urumqi, Xinjiang, 830001, People's Republic of China, Email xjmnlixun@163.com

Objective: This study aimed to develop and validate a machine learning-based model for predicting systemic inflammatory response syndrome (SIRS) in pediatric patients undergoing percutaneous nephrolithotripsy (PCNL) and to establish a prediction platform specifically tailored for this population.

Methods: We retrospectively analyzed clinical data from 410 pediatric patients who underwent PCNL at the People's Hospital of Xinjiang Uygur Autonomous Region between January 2013 and September 2024. The dataset was split into training and validation sets using a 7:3 ratio based on positive samples. The Synthetic Minority Over-sampling Technique (SMOTE) was applied to overcome class imbalance in the training set, while feature selection was performed using a combination of LASSO regression and Boruta algorithms. Eight advanced machine learning algorithms were employed to construct predictive models. The best-performing model was selected based on multiple performance metrics. Additionally, we validated an existing adult model to assess its effectiveness in the pediatric population and compared it with our model. Shapley Additive Explanations (SHAP) analysis was utilized to determine feature importance and model decision basis. Finally, we developed a prediction platform specifically for pediatric patients.

Results: The postoperative SIRS incidence was 20.24%. The LightGBM algorithm demonstrated superior predictive performance, achieving an area under the curve (AUC) of 0.8576 and an F1 score of 0.6154. The existing adult models showed lower predictive accuracy in the pediatric cohort (AUC values of 0.7420 and 0.7053). Analysis of SHAP values indicated that operation time, stone burden, preoperative hemoglobin, preoperative monocyte count, and hydronephrosis were the five most critical features affecting predictions. We established a prediction platform specifically designed for the pediatric population.

Conclusion: The LightGBM-based model effectively predicts postoperative SIRS in pediatric PCNL patients, providing a tailored tool for this population. The online prediction platform might be useful to guide clinical decision making.

Keywords: pediatric, percutaneous nephrolithotripsy, kidney stones, systemic inflammatory response syndrome, machine learning, clinical prediction platform

Introduction

While pediatric kidney stones remain comparatively uncommon, their global incidence demonstrates an upward trend annually, leading to considerable healthcare-associated costs.[1–3]The treatment and management of pediatric patients with kidney stones is more complex than that of adults due to several factors including high recurrence rates, co-existing metabolic abnormalities, and anatomical differences in the kidney and perirenal tissues.[4,5] These factors often necessitate frequent surgical interventions. The miniaturization of endoscopic instruments used for percutaneous nephrolithotripsy (PCNL) has facilitated its increasing application in the treatment of pediatric kidney stones.[6,7] The International Alliance of Urolithiasis (IAU) guidelines recommend PCNL as the primary surgical procedure for pediatric patients with stones larger than 2 cm or complex upper urinary tract stones.[8]

Received: 21 January 2025
Accepted: 21 May 2025
Published: 30 May 2025

Pediatric PCNL has gained widespread acceptance among urologists for treating kidney stones in pediatric patients due to its small dilatation channel, high safety profile and high stone-free rate.[9] However, postoperative complications, especially Systemic inflammatory response syndrome (SIRS), should not be ignored. SIRS, a systemic inflammatory response caused by severe infections, trauma, and surgical procedures, is strongly associated with poor prognosis and significantly increased mortality risk.[10] SIRS is one of the most common complications after PCNL, maintains a high incidence (9.8–43%) despite preoperative antibiotics.[11] As the initial stage in sepsis progression, it is closely linked to its development. Furthermore, sepsis is one of the leading causes of perioperative mortality after PCNL, with mortality rates ranging from 20% to 42%.[12,13] Therefore, early identification of high-risk pediatric patients during the "therapeutic window" between SIRS onset and sepsis development and timely intervention are key to reducing the incidence of sepsis and mortality after PCNL. However, it is noteworthy that although the study of post-PCNL SIRS is more mature in adults, there is a virtual void of similar studies in the pediatric population.[12–15]

Machine learning has been extensively applied in various areas of the biomedical field, including disease diagnosis, prognosis prediction, and medical image analysis.[16–18] In comparison to traditional regression algorithms, machine learning excels at identifying nonlinear relationships and addressing high-dimensional spatial problems in data, achieving high accuracy and strong generalization capabilities. Pediatric patients present unique challenges including smaller sample sizes, age-dependent immune responses, and threshold effects in surgical stress reactions that conventional linear models cannot adequately capture. Li et al and Zhang et al had successfully developed prediction models for SIRS after PCNL in adults using machine learning methods; however, their predictive performance has not been validated in pediatric patients.[13,19] Therefore, our study aimed to compare the predictive performance of multiple machine learning algorithms for SIRS after pediatric PCNL, utilizing preoperative and surgery-related clinical data. Additionally, we sought to identify the key predictive factors and compare the performance of our model with existing adult models by directly evaluate two established adult PCNL-SIRS models in our pediatric cohort using identical validation protocols. Ultimately, we aimed to develop a straightforward and reliable prediction platform for this population, which may provide a scientific basis for urologists to enhance perioperative management.

Methods

Study Population

We retrospectively analyzed clinical data from 463 pediatric patients (aged ≤14 years) with non-contrast CT confirmed kidney stones who underwent primary PCNL at the Department of Urology, People's Hospital of Xinjiang Uygur Autonomous Region between January 2013 and September 2024. We excluded the following pediatric patients to minimize confounding factors affecting the occurrence of postoperative SIRS: Preoperative presence of SIRS or other serious infectious disease; prior kidney surgery on the affected side; history of bilateral PCNL during study period; urological malformations such as polycystic kidneys, horseshoe kidneys or isolated kidneys; with tumors, blood system or immune system diseases; and with incomplete clinical data or missing follow up after operation. This study followed the principles of the Declaration of Helsinki and was conducted in accordance with the ethical standards of the Medical Ethics Committee of our hospital. The research flowchart is shown in (Figure 1)

Data Collection

We collected data based on previous relevant studies, clinical experience, and data accessibility, demographic characteristics included age, gender, and body mass index (BMI). Preoperative data included temperature, heart rate, respiratory rate, white blood cell count (WBC), hemoglobin (HB), neutrophils (N), lymphocytes (L), monocytes (M), platelets (PLT), hematocrit (HCT), neutrophil-lymphocyte ratio (NLR), platelet-lymphocyte ratio (PLR), lymphocyte-monocyte ratio (LMR), systemic immune inflammatory index (SII), prognostic nutritional index (PNI), urine nitrite, urine WBC, urine culture, serum creatinine, urea nitrogen, uric acid, cystatin, albumin, fibrinogen, stone burden (length × width × π × 0.25), hydronephrosis, and presence of staghorn stones. Patients with positive preoperative urine culture, positive urine nitrite, and positive urine WBC underwent surgery after negative conversion. All patients received prophylactic antibiotics preoperatively. Surgery-related data included the location, size, and number of channels, whether a nephrostomy tube was placed, operation time, and

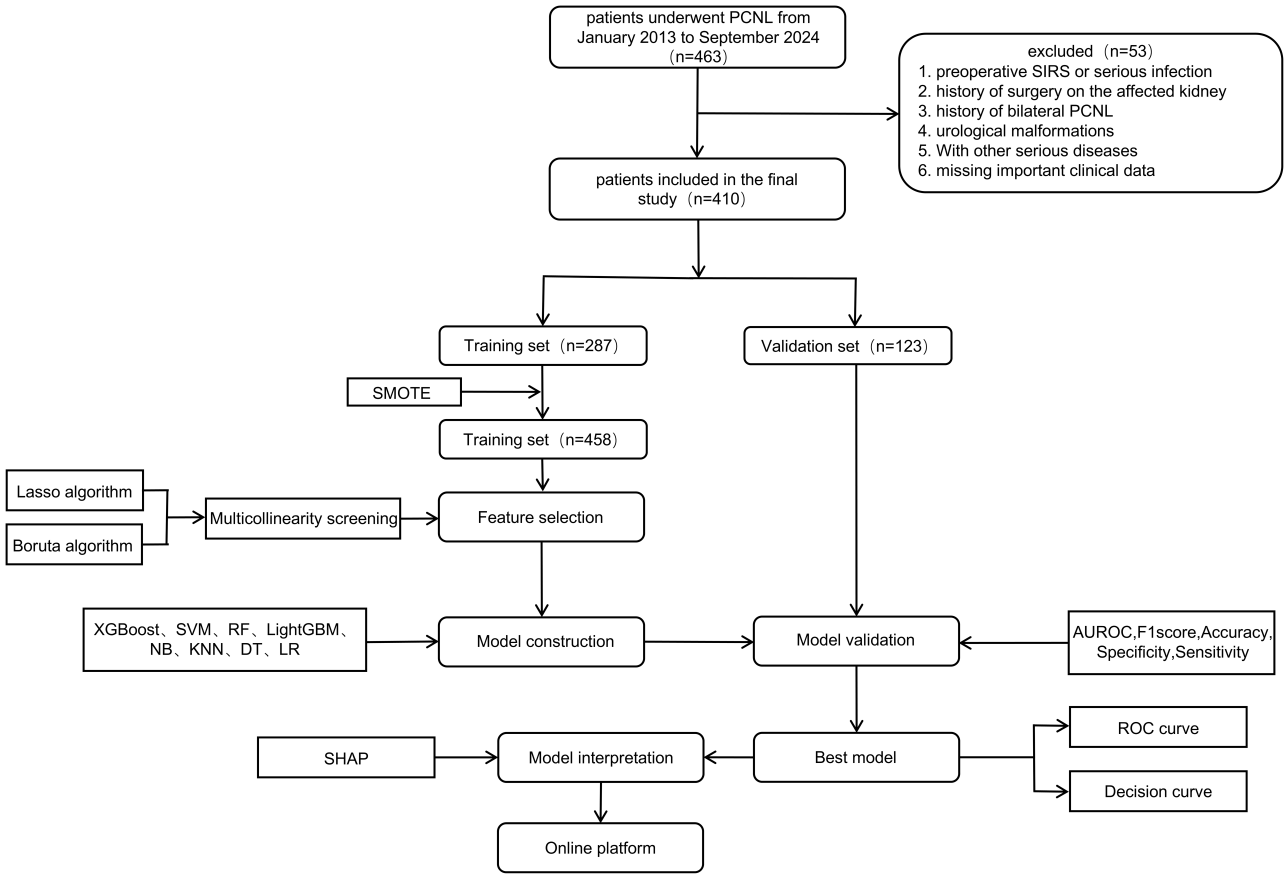

Figure 1 Research flowchart.
Abbreviations: PCNL, percutaneous nephrolithotripsy; SIRS, systemic inflammatory response syndrome; SMOTE, Synthetic Minority Over-sampling Technique; Light; GBM, Light Gradient Boosting Machine; XGBoost, EXtreme Gradient Boosting; LR, Logistic Regression; RF, Random Forest; SVM, Support Vector Machine; KNN, K-Nearest Neighbours; NB, Naive Bayes; DT, Decision Tree; AUROC, Area Under the Receiver Operating Characteristic Curve; SHAP, Shapley Additive Explanations.

whether blood transfusion was required. Postoperative data were uniformly measured at 6 a.m. on the first day after surgery and included WBC, temperature, heart rate, respiratory rate, and arterial carbon dioxide partial pressure (PCO2).

SIRS is diagnosed in pediatric patients who meet at least two of the following four criteria, with one criterion being an abnormal temperature or leukocyte count: 1. temperature >38.5°C or <36°C; 2. mean heart rate >2 standard deviations (SD) above the normal range for age or mean heart rate <10th percentile for age; 3. mean respiratory rate >2 SD above the normal range for age; 4. leukocyte count that is either elevated or depressed for age (excluding chemotherapy-induced leukopenia) or >10% immature neutrophils.[20]

Data Preprocessing

We employed random sampling of positive instances to divide the patients into a training set (287 patients) and a validation set (123 patients), maintaining a 7:3 ratio. This method ensures that positive samples are adequately represented in both sets. Due to the low percentage of patients who developed postoperative SIRS, we applied the Synthetic Minority Over-sampling Technique (SMOTE) to the training set. this approach aims to enhance model learning and mitigate performance bias from class imbalance.[21] We applied Min-Max normalization to continuous variables and one-hot encoding to categorical variables based on the reference intervals for various age groups in children. (Table S1)

Feature Selection

First, we utilized the random forest-based Boruta algorithm and LASSO regression for feature selection on the over-sampled training dataset. By selecting features identified as important by both algorithms, we enhanced the credibility of

https://doi.org/10.2147/JIR.S518631

the feature selection process.[22] Subsequently, to ensure there was no collinearity among the selected features, we performed a collinearity screening. Collinearity indicates a high correlation among multiple predictor variables, which can result in unstable model estimates and difficulties in interpretation. We calculated the Variance Inflation Factor (VIF) for the features to identify and exclude those with collinearity issues, thus ensuring the model's stability and reliability. Through this comprehensive process, we ultimately identified the feature variables utilized for model construction.

Model Construction

We used eight machine learning methods: Random Forest (RF), Extreme Gradient Boosting (XGBoost), Logistic Regression (LR), K-Nearest Neighbors (KNN), Light Gradient Boosting Machine (LightGBM), Decision Tree (DT), Support Vector Machine (SVM), and Naive Bayes (NB). These algorithms are widely used in clinical data analysis due to their effectiveness in handling complex datasets and providing high predictive accuracy.[18,23] Additionally, we assessed the applicability of adult models in the pediatric population and compared their performance with our model.

RF is an ensemble learning method that enhances model stability and accuracy by constructing multiple decision trees and aggregating their predictions through voting or averaging. RF can effectively handle high-dimensional data and is notably resistant to overfitting.

XGBoost is an efficient gradient boosting framework that minimizes regularized objective functions through the iterative construction of tree models. It optimizes the model's predictive performance while controlling for overfitting.

LR is a linear model used to predict the probability of a classification outcome, converting the model's output into probability values using a logistic function. Its strengths include the model's simplicity and the clear statistical significance of its parameters.

KNN is based on a distance metric and classifies instances by identifying the K nearest neighbors in the training set to a new sample. The advantage of KNN lies in the algorithm's simplicity and its adaptability to nonlinear problems.

LightGBM is a gradient boosting framework optimized with a histogram-based algorithm to enhance the learning efficiency of tree models. Its advantage lies in reducing computational complexity and accelerating model training.

DT constructs a model by recursively partitioning the feature space, where each node represents a decision rule for a feature, making the model intuitive and easy to interpret.

SVM distinguishes between different classes of data points by identifying an optimal hyperplane in the feature space. Its advantages include strong generalization capabilities in high-dimensional spaces and small sample cases, as well as adaptability to nonlinear problems.

NB is based on Bayes' theorem, assuming that features are independent of one another and predicting categories using conditional probabilities of the features. Its advantages lie in the algorithm's simplicity and high efficiency.

We employed a grid search method for hyperparameter optimization of each machine learning model, along with 5-fold cross-validation to assess each hyperparameter combination.

Model Validation

We conducted a comprehensive evaluation of each model using a series of key performance metrics, including Area Under the Receiver Operating Characteristic Curve (AUROC), Accuracy, F1-Score, Specificity, and Sensitivity, ultimately selecting the model with the best predictive performance as the final model. These metrics provide a comprehensive reflection of the models' predictive performance and allow us to evaluate them from multiple perspectives. We conducted an in-depth analysis of the predictive results for the best model using the Shapley Additive Explanations (SHAP) method. This method accurately measures the specific contribution of each feature to the model's predictions by assigning a quantitative score to each feature.[24]

Additional Statistical Methods

In this study, we used R version 4.4.2 and SPSS version 29.0 for statistical analysis and data visualization. Continuous variables that conformed to normal distribution were expressed as mean ± standard deviation and differences between groups were assessed using t-tests, continuous variables that did not conform to normal distribution were expressed as median and quartiles, and differences between groups were assessed using Mann–Whitney *U*-tests. Categorical variables were expressed

as frequencies and percentages, with differences between groups assessed using the chi-square test or Fisher's exact test. We considered a two-tailed P-value of <0.05 as the significance threshold for determining statistical differences.

Results

Population Characteristics

We ultimately included 410 eligible pediatric patients, with a mean age of 6.44 ± 3.94 years, among whom 237 (57.8%) were boys. Postoperatively, 83 patients developed SIRS, resulting in an incidence rate of 20.24%. Based on the occurrence of SIRS postoperatively, we divided the patients into two groups. The two groups showed significant differences across multiple clinical parameters. Patients with SIRS had larger stone burdens (median 207.35 vs 123.21 mm², p<0.0001), longer operation times (95 vs 75 min, p<0.0001), and higher rates of hydronephrosis (60.24% vs 22.94%, p<0.0001) and staghorn calculi (48.19% vs 12.23%, p<0.0001). Urinary markers also differed significantly, with SIRS patients exhibiting more frequent positive urine cultures (38.55% vs 23.24%, p=0.0047), nitrites (33.73% vs 14.07%, p<0.0001), and leukocytes (77.11% vs 62.39%, p=0.0118). Procedural characteristics revealed SIRS cases more often required multiple access channels (14.46% vs 3.67%, p=0.0002) and nephrostomy tube placement (75.90% vs 59.63%, p=0.0061). The baseline information of the patients is shown in (Table 1).

Table 1 Clinical Characteristics of Pediatric Patients with and Without Postoperative SIRS

Variables	Total (n=410)	Without SIRS (n=327)	With SIRS (n=83)	P-value
Age (years)	6 (3–10)	6 (3–10)	6 (2.5–10.5)	0.8346
Stone burden (mm^2)	127.43 (84.31–202.95)	123.21 (84.16–174.55)	207.35 (87.96–410.33)	<0.0001
Operation time (min)	80 (70–95)	75 (70–95)	95 (82.5–105)	<0.0001
Preoperative WBC (10^9/L)	8.5 (6.6–11)	8.43 (6.6–10.93)	8.53 (6.56–11.95)	0.5392
Preoperative N (10^9/L)	3.67 (2.72–5.08)	3.64 (2.71–5.06)	3.81 (2.78–5.17)	0.6771
Preoperative L (10^9/L)	409.38 (261.15–600.78)	402.93 (260.76–607.35)	422.44 (276.98–563.32)	0.9396
Preoperative M (10^9/L)	1.15 (0.73–1.67)	1.18 (0.74–1.7)	1.11 (0.72–1.59)	0.5172
Preoperative SII	3.18 (2.35–4.74)	3.13 (2.36–4.6)	3.33 (2.37–5.41)	0.3498
Preoperative NLR	107.83 (78.34–142.38)	108.47 (79.25–143.67)	106.55 (77.06–139.94)	0.5344
Preoperative PLR	6.51 (4.86–9.06)	6.45 (4.87–8.99)	6.74 (4.87–9.31)	0.4930
Preoperative LMR	58.24 (53.37–65.96)	58 (53.24–65.12)	60.3 (53.87–68.22)	0.1775
Preoperative PNI	0.51 (0.38–0.72)	0.51 (0.38–0.71)	0.54 (0.36–0.75)	0.7910
Preoperative PLT (10^9/L)	359 (296–432.5)	355 (294–425)	370 (306.5–475.5)	0.1920
Preoperative HB (g/L)	121.08±13.28	121.64±12.88	118.88±14.61	0.1181
Preoperative HCT	0.37±0.04	0.38±0.04	0.37±0.04	0.0743
Serum creatinine (μmol/L)	32.67 (25.34–40.15)	32 (25.15–39.5)	34.32 (25.81–42.53)	0.2561
Urea nitrogen (mmol/L)	4.83±1.47	4.81±1.46	4.95±1.51	0.4382
Serum uric acid (μmol/L)	228.23±63.82	226.85±64.77	233.67±60	0.3642
Serum cystatin (mg/L)	0.9 (0.78–1.07)	0.92 (0.78–1.09)	0.86 (0.78–1.02)	0.2221
Serum albumin (g/L)	41.8±3.38	41.78±3.34	41.87±3.56	0.8335

(*Continued*)

https://doi.org/10.2147/JIR.S518631

Table 1 (Continued).

Variables	Total (n=410)	Without SIRS (n=327)	With SIRS (n=83)	P-value
Serum fibrinogen (g/L)	2.63 (2.17–3.26)	2.61 (2.16–3.12)	2.76 (2.34–3.74)	0.0697
BMI (kg/m^2)	15.97 (14.58–17.65)	15.87 (14.53–17.35)	16.33 (14.91–18.07)	0.1601
Gender (%)				0.7992
Female	173 (42.20)	139 (42.51)	34 (40.96)	
Male	237 (57.80)	188 (57.49)	49 (59.04)	
Urine culture (%)				0.0047
Negative	302 (73.66)	251 (76.76)	51 (61.45)	
Positive	108 (26.34)	76 (23.24)	32 (38.55)	
Hydronephrosis (%)				<0.0001
No	285 (69.51)	252 (77.06)	33 (39.76)	
Yes	125 (30.49)	75 (22.94)	50 (60.24)	
Stone side (%)				0.2378
Left	179 (43.66)	138 (42.20)	41 (49.40)	
Right	231 (56.34)	189 (57.80)	42 (50.60)	
Channel location (%)				0.0640
Upper calyces	93 (22.68)	82 (25.08)	11 (13.25)	
Median calyces	263 (64.15)	202 (61.77)	61 (73.49)	
Lower calyces	54 (13.17)	43 (13.15)	11 (13.25)	
Staghorn stones (%)				<0.0001
No	330 (80.49)	287 (87.77)	43 (51.81)	
Yes	80 (19.51)	40 (12.23)	40 (48.19)	
Urine nitrite (%)				<0.0001
Negative	336 (81.95)	281 (85.93)	55 (66.27)	
Positive	74 (18.05)	46 (14.07)	28 (33.73)	
Urine WBC(%)				0.0118
Negative	142 (34.63)	123 (37.61)	19 (22.89)	
Positive	268 (65.37)	204 (62.39)	64 (77.11)	
Channel size (%)				0.0566
Ultra-micro channel	197 (48.05)	160 (48.93)	37 (44.58)	
Micro channel	203 (49.51)	162 (49.54)	41 (49.40)	
Standard channel	10 (2.44)	5 (1.53)	5 (6.02)	

(*Continued*)

Table 1 (Continued).

Variables	Total (n=410)	Without SIRS (n=327)	With SIRS (n=83)	P-value
Number of channels (%)				0.0002
1	386 (94.15)	315 (96.33)	71 (85.54)	
2	24 (5.85)	12 (3.67)	12 (14.46)	
Nephrostomy tube indwelled (%)				0.0061
No	152 (37.07)	132 (40.37)	20 (24.10)	
Yes	258 (62.93)	195 (59.63)	63 (75.90)	
Blood transfusion (%)				0.0595
No	384 (93.66)	310 (94.80)	74 (89.16)	
Yes	26 (6.34)	17 (5.20)	9 (10.84)	

Abbreviations: WBC, white blood cell; N, neutrophil; L, lymphocyte; M, monocyte; SII, Systemic immune inflammatory Index; NLR, neutrophil-lymphocyte ratio; PLR, platelet-lymphocyte ratio; LMR, lymphocyte-monocyte ratio; PNI, Prognostic nutritional Index; PLT, platelet; HB, hemoglobin; HCT, hematocrit; BMI, body mass index.

Feature Selection

Our feature selection process employed a dual-algorithm approach (Figure 2): LASSO regression with ten-fold cross-validation reduced 34 initial variables to 15 non-zero coefficients using the λ.1se criterion (vertical dotted line at 1 standard error above minimum cross-validated error in Figure 2A), which provides the simplest model within one standard error of the optimal fit. Figure 2B illustrates how feature coefficients evolved across λ values. The Boruta algorithm (Figure 2C) independently confirmed 29 important variables significantly exceeding shadow features' importance threshold. Figure 2D revealed overlapping variables from both methods. We conducted a collinearity screening of the features (Table 2), revealing that all features had a variance inflation factor (VIF) of <5, indicating no significant collinearity issues. Given comparable predictive performance between the full feature set model and the top 10-feature model, we ultimately selected the top 10 features based on their importance ranking to optimize prediction speed and facilitate clinical implementation (Table 2). [18] These features included: operation time, stone burden, staghorn stones, hydronephrosis, hemoglobin, hematocrit, neutrophils, lymphocytes, monocytes, and SII.

Model Performance

SMOTE oversampling was exclusively applied to the training set (n=287) to create a balanced subset (n=458), while the validation set (n=123) retained original real-case proportions for unbiased evaluation. The results of the model performance evaluation are presented in (Table 3 and Figure 3B). The ROC curves and areas under the curve are shown in (Figure 3A). The results indicate that LightGBM performed the best in predicting SIRS after pediatric PCNL, achieving an AUC of 0.8758 and an F1 score of 0.6275, thus outperforming the other models. The decision curve analysis demonstrates that the model achieves good net benefit within a threshold probability range of 0.05 to 0.70 (Figure 3C). Additionally, we validated the applicability of two existing adult models in the pediatric population (AUC: 0.7420 and 0.7053, respectively), and the results indicated that our model outperformed the adult models in predicting SIRS after pediatric PCNL (Figure 3D).

Model Interpretation

We employed the SHAP method to quantify the contribution of each feature to the model's predictions. We visually presented the SHAP values of various features (Figure 4A), where each point corresponds to a sample, and its position indicates the SHAP value for that sample on a specific feature. The color gradient from yellow to purple represents the magnitude of the feature value for each sample, thereby intuitively revealing the positive or negative impact of the feature

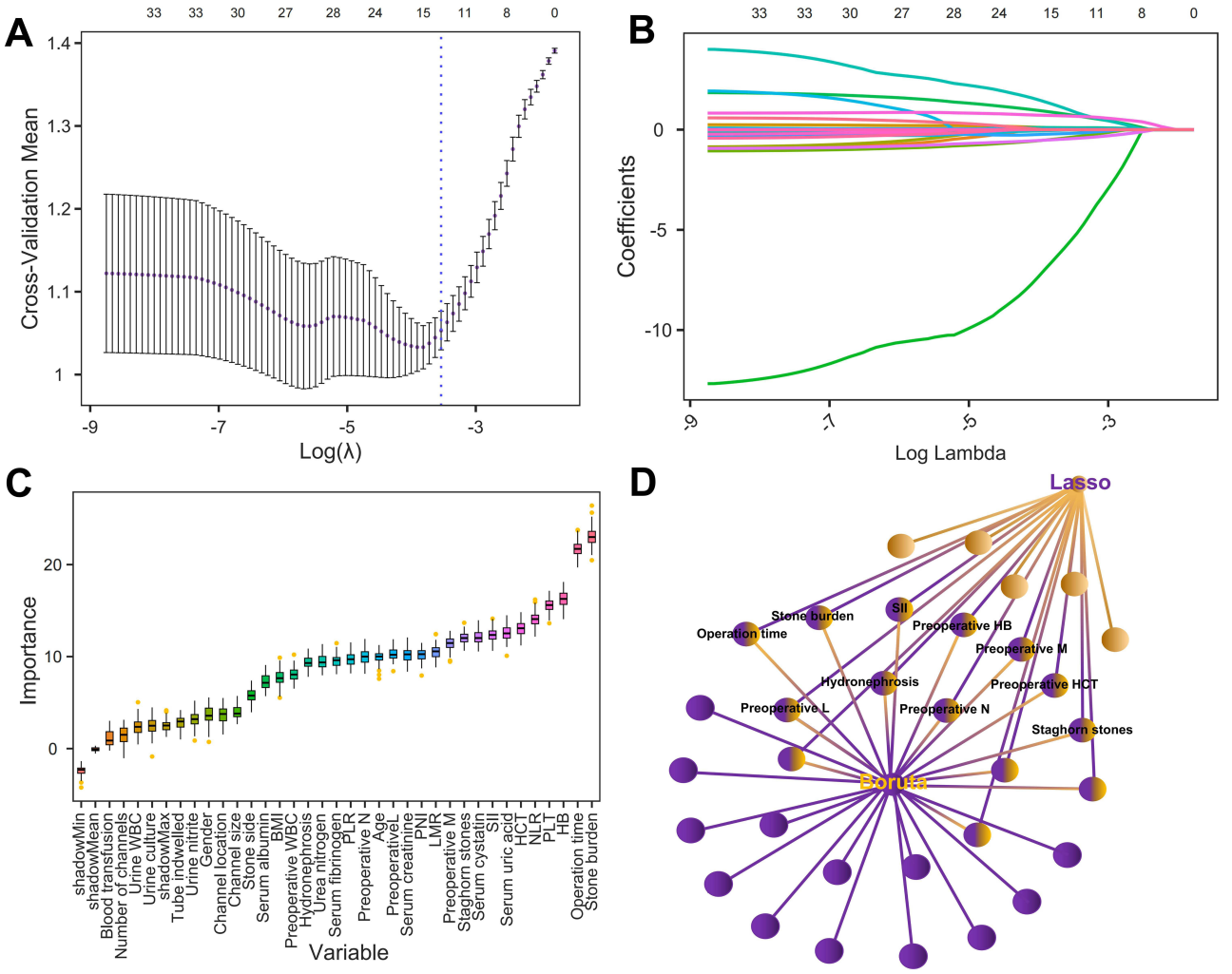

Figure 2 Results of feature screening. (**A**) Feature screening based on the LASSO regression, the dashed line indicating the lambda value for the model where the evaluation metrics are in the range of the best value by one standard error (lambda.1se). (**B**) LASSO regression screening feature trajectories. (**C**) Boruta feature importance analysis. (**D**) common features between Boruta and LASSO.

on the model's predictions. For example, individuals with longer operation times were more likely to develop postoperative SIRS compared to those with shorter operation times, and conversely, individuals with lower hemoglobin were more likely to develop postoperative SIRS compared to those with higher hemoglobin. Furthermore, we constructed a bar chart illustrating feature importance rankings (Figure 4B), assessing the significance of each feature to the model's predictions by calculating the mean absolute values of their SHAP values. The top five identified features were operation time, stone burden, preoperative hemoglobin, preoperative monocyte count, and hydronephrosis. To understand the model's decision-making process at the individual level, we conducted a detailed interpretability analysis of representative samples (Figure 4C and D).

Construction of Web Platform

We developed a web-based prediction platform using the LightGBM algorithm to assist clinicians in predicting the risk of postoperative SIRS in pediatric patients undergoing PCNL (https://sirspredict.shinyapps.io/lightgbm/). By entering the relevant values for each variable in the predictive variables panel, users can assess the risk of postoperative SIRS and visualize the contributions of each factor to the outcome, thereby enabling targeted preoperative prophylaxis (Figure 5).

Table 2 Variable Variance Inflation Factors and Rank of Importance

Variables	VIF	Importance
Stone burden	3.26	30.34
Operation time	1.82	26.57
Preoperative HB	2.65	20.05
Preoperative HCT	2.77	17.51
Preoperative SII	4.04	17.15
Preoperative L	2.67	16.37
Preoperative M	2.37	16.25
Staghorn stones	2.50	13.52
Hydronephrosis	1.23	13.26
Preoperative N	3.96	12.98
Urea nitrogen	1.12	11.93
BMI	1.15	10.51
Stone side	1.03	7.32
Gender	1.12	6.10
Channel size	1.24	5.72

Abbreviations: VIF, Variance Inflation Factors; HB, hemoglobin; HCT, hematocrit; SII, Systemic immune inflammatory Index; L, lymphocyte; M, monocyte; N, neutrophil; BMI, body mass index.

Table 3 Performance Evaluation Metrics of Eight Machine Learning Models and Adult Models in the Test Set

Model	Accuracy	F1-Score	AUC(95 CI)	Specificity	Sensitivity
LightGBM	0.854	0.654	0.872(0.799–0.945)	0.898	0.68
XGBoost	0.837	0.615	0.851(0.762–0.940)	0.888	0.64
LR	0.756	0.531	0.800(0.694–0.907)	0.776	0.68
RF	0.764	0.491	0.747(0.641–0.854)	0.816	0.56
SVM	0.821	0.421	0.698(0.559–0.838)	0.949	0.32
KNN	0.683	0.400	0.678(0.563–0.792)	0.725	0.52
NB	0.602	0.380	0.674(0.545–0.803)	0.602	0.60
DT	0.659	0.300	0.614(0.486–0.741)	0.735	0.36
Adult model1	0.715	0.386	0.742(0.631–0.853)	0.786	0.44
Adult model2	0.821	0.421	0.705(0.578–0.833)	0.949	0.32

Abbreviations: AUC, area under the curve; LightGBM, Light Gradient Boosting Machine; XGBoost, EXtreme Gradient Boosting; LR, Logistic Regression; RF, Random Forest; SVM, Support Vector Machine; KNN, K-Nearest Neighbours; NB, Naive Bayes; DT, Decision Tree.

https://doi.org/10.2147/JIR.S518631

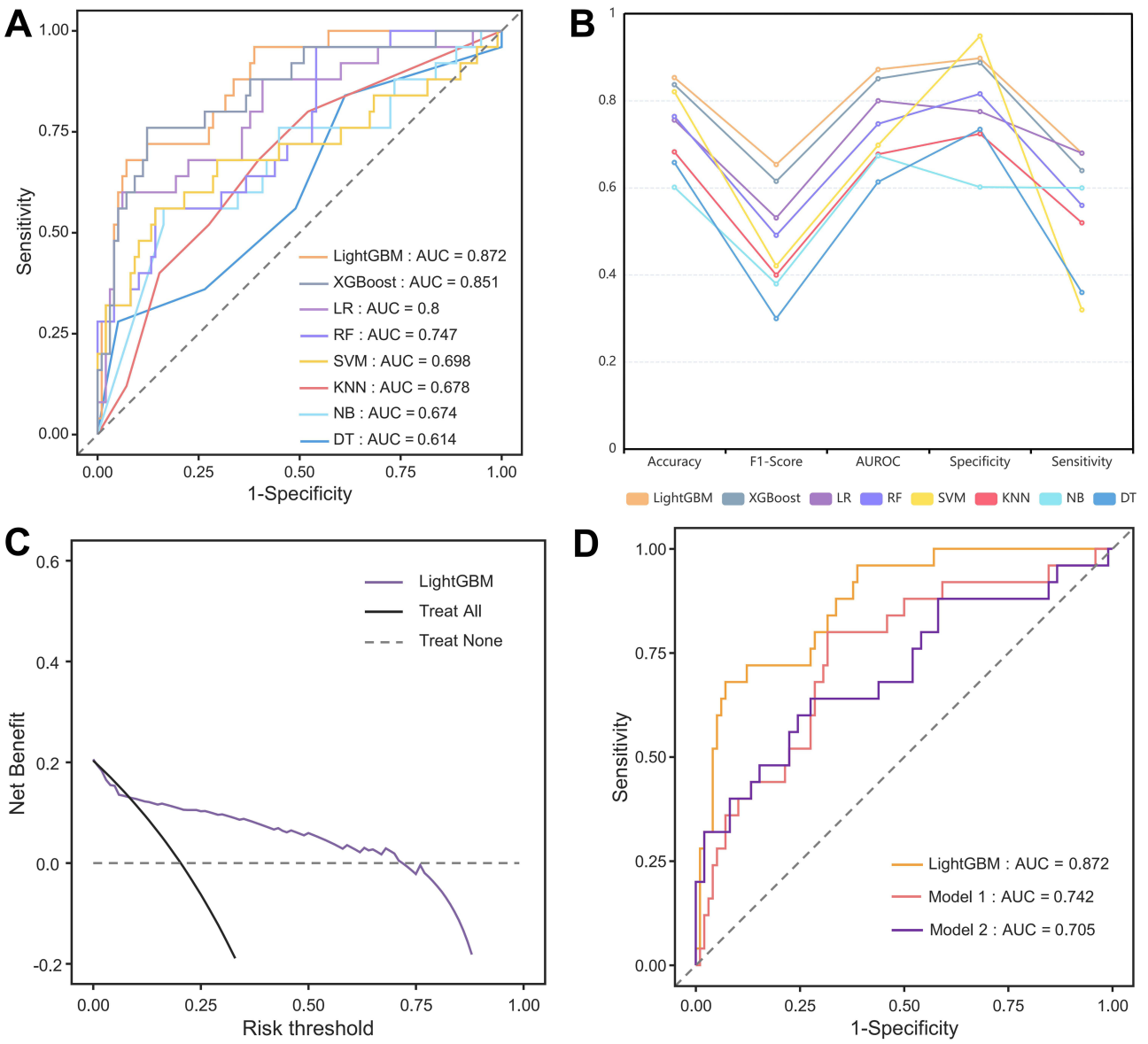

Figure 3 The performance and comparison of different models. (**A**) ROC curve for the validation set. (**B**) Evaluation metrics for the validation set. (**C**) Decision curve analysis for the validation set. (**D**) ROC curve for comparison with adult models.

Discussion

The use of PCNL in pediatric patients has become increasingly widespread. As surgical techniques continue to advance, postoperative infections have become the main concern regarding complications. SIRS is among the most common complications after PCNL and can be difficult to detect early.[25,26] If left untreated, SIRS may progress to sepsis or multi-organ dysfunction.[19] Although multiple tools exist for predicting SIRS after PCNL in adults, our study indicates that these methods are less effective in pediatric patients. Consequently, developing and validating a predictive model for SIRS after PCNL in pediatric patients, along with creating an accessible online prediction platform for individual risk assessment, is of significant clinical importance. Such model can be integrated into clinical data systems to automatically predict the risk of postoperative SIRS. The advent of artificial intelligence and machine learning has enabled the development of such personalized systems. To our knowledge, our study is the first attempt to utilize machine learning algorithms to develop a predictive model for SIRS after PCNL in pediatric patients.

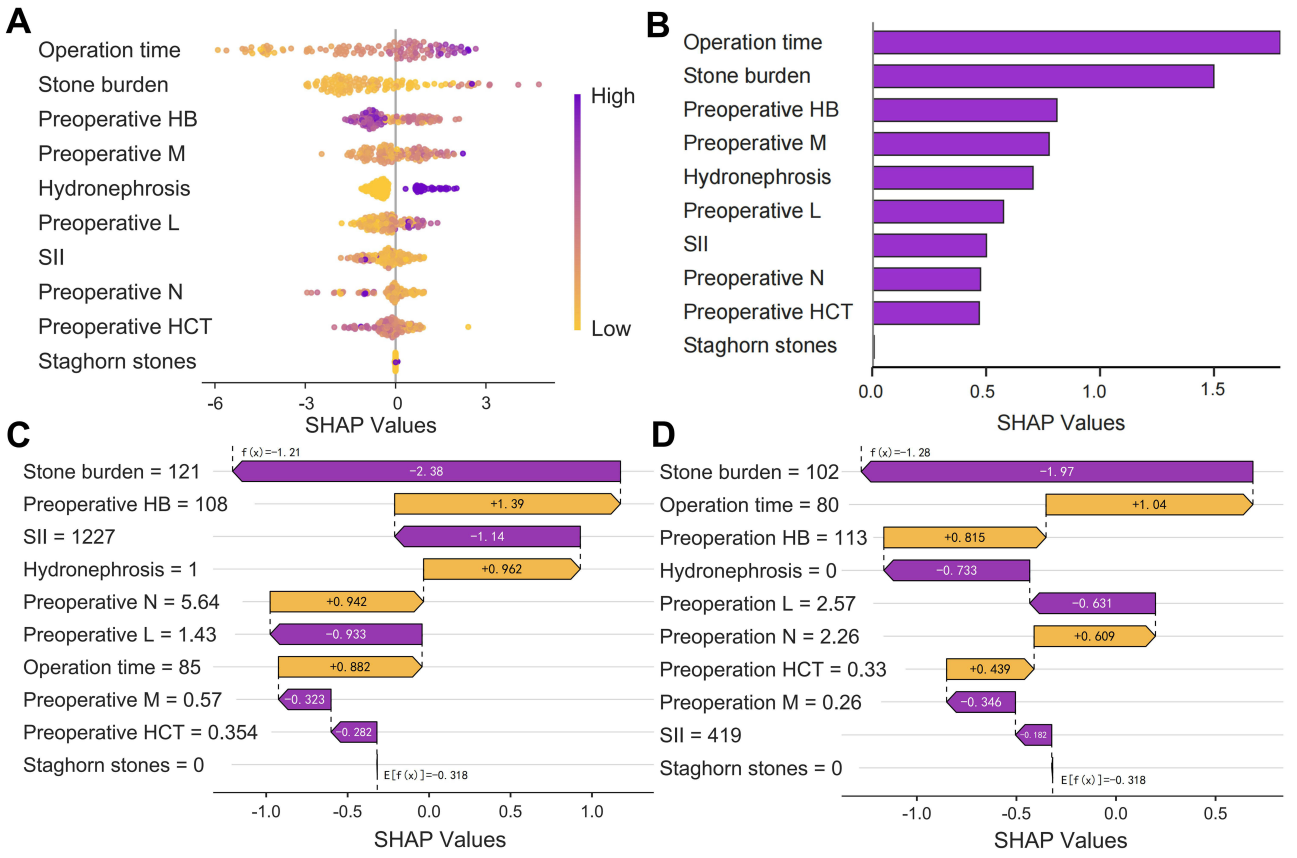

Figure 4 Interpretability analysis of LightGBM model. (**A**) SHAP Beeswarm Plot illustrating the contribution of each feature to the model's predictions. Each point represents an instance, with colors indicating the feature value. (**B**) Importance Ranking Plot of Features showing the relative importance of each feature in predicting outcomes. (**C**) (**D**) Interpretability Analysis of Independent Sample demonstrating the model's performance and feature contributions on a separate sample.

Notable differences emerged between our findings and established adult PCNL-SIRS prediction models. While prior adult studies identified preoperative urine culture positivity and perioperative platelet decline as primary predictors, our pediatric model highlighted operation time as the dominant risk factor. Although Previous studies confirmed that prolonged operation time is a significant risk factor for SIRS after PCNL in adults. Our findings indicate that this risk may be even greater in the pediatric population.[14,27] In our study, operation time was the most significantly correlated factor with the occurrence of postoperative SIRS. Extended operation time often leads to increased mechanical pressure on the renal pelvis, a higher risk of injury due to prolonged manipulation, and extended anesthesia duration. These factors may cause more severe damage to the fragile kidneys of pediatric patients compared to adults.[28] Elevated pressure in the renal pelvis can facilitate bacterial entry into circulation through dilated mucosa, thus increasing the risk of infection. Additionally, elevated pressure may affect local blood circulation, exacerbate localized inflammatory responses, and trigger systemic inflammation. Prolonged endoscopic procedures increase the risk of renal tissue damage, including laser-induced thermal injuries and direct mucosal damage from the endoscope. These injuries can induce local inflammation, release inflammatory mediators, attract immune cells, and intensify inflammation.[29,30] Extended anesthesia duration may result in renal ischemia-reperfusion injury, triggering a cascade of oxidative stress responses and the release of inflammatory mediators, thereby increasing the risk of SIRS.[31,32] Therefore, controlling operation time is crucial to reducing the incidence of SIRS after PCNL.

Stone burden is a significant risk factor for SIRS after PCNL, with its contribution to the model ranking second only to operation time. A larger stone burden typically indicates more complex surgical procedures and prolonged lithotripsy time, which increase the risk of surgical trauma and may trigger inflammatory responses. Additionally, large stones can easily obstruct the urinary outflow tract, resulting in hydronephrosis and prolonged urine retention in the kidneys. This condition increases the risk of bacterial proliferation and subsequent infection, while also hindering accurate assessment of potential infections through urine tests.[19] As a result, it may mislead preoperative anti-infective strategies and elevate the risk of

https://doi.org/10.2147/JIR.S518631

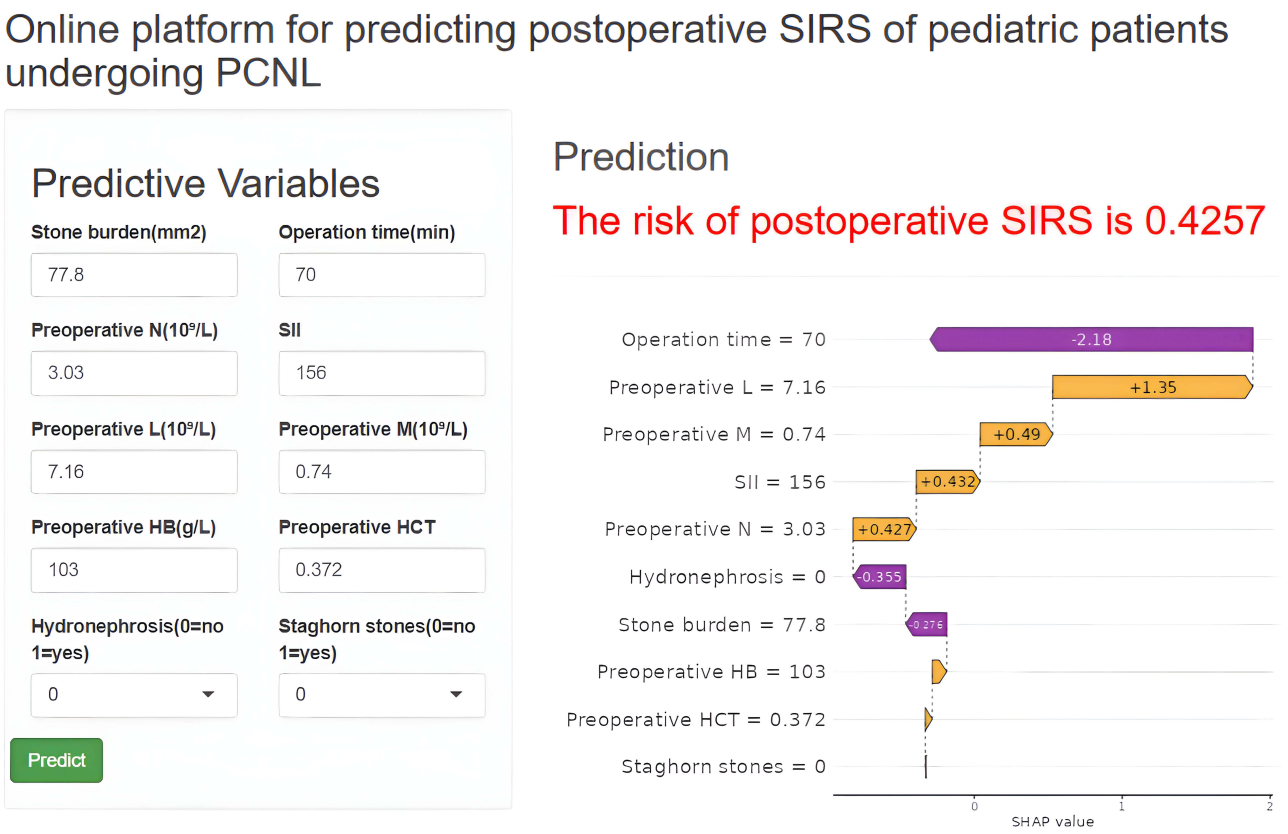

Figure 5 Online prediction platform based on LightGBM algorithm for predicting SIRS after pediatric PCNL.

postoperative SIRS. Larger stones may suggest a prolonged presence in the kidneys, leading to bacterial colonization and an increased risk of inflammatory responses. Therefore, special attention should be given to these pediatric patients. An intraoperative urine culture of the renal pelvis can be performed to inform subsequent anti-infective strategies.[33,34]

Hemoglobin, the primary oxygen carrier, directly affects tissue oxygenation levels. Low hemoglobin levels can cause tissue hypoxia, which exacerbates inflammatory responses. In the context of surgical trauma, hypoxia may further activate inflammatory pathways, thus increasing the risk of SIRS.[35] Numerous studies indicated that hemoglobin and its derivatives significantly modulate immune response, indicating that hemoglobin is not only involved in oxygen transport but may also play a role in the body's immune responses. Additionally, hemoglobin reduces oxidative stress, which helps maintain cellular function and protects against bacterial invasion.[36,37] In summary, the potential mechanisms linking preoperative hemoglobin levels to SIRS after PCNL may include oxygenation status, inflammatory responses, immune modulation, and oxidative stress, among other factors. These findings emphasize the importance of preoperative assessment of hemoglobin levels.

Monocytes, crucial components of the innate immune response, are pivotal in the development of SIRS. Surgical trauma and tissue injury activate monocytes, resulting in the release of various inflammatory mediators, including interleukin-6 (IL-6), which initiates and amplifies the inflammatory response. Moreover, activated monocytes participate in the synthesis and expression of procoagulant factors, potentially leading to hypercoagulability and exacerbating the pathophysiological processes associated with SIRS.[38,39] This multifaceted synergistic effect may positions monocytes as a driving force in the onset and progression of SIRS.

In summary, the interplay among the aforementioned risk factors underscores the complexity of managing pediatric patients undergoing PCNL. Each of these factors contributes to an elevated overall risk of postoperative SIRS, emphasizing the necessity for meticulous preoperative assessment and postoperative monitoring. Understanding these associations can assist clinicians in identifying high-risk patients who are at risk of developing SIRS and in implementing targeted preoperative optimization and postoperative management strategies to reduce the incidence of postoperative SIRS, thereby enhancing the surgical safety of this vulnerable population.

While this study offers valuable insights, it is not without limitations. This is a single-center, retrospective study that may be subject to selection bias, and the external validity of the model has yet to be validated in an independent sample. In the future, we plan to validate the predictive performance of the model further through multi-center, prospective studies and to explore additional potential risk factors to enhance both the predictive accuracy and clinical applicability of the model. Additionally, we will examine the applicability of the model across different clinical settings, as well as ways to translate these findings into practical clinical guidelines aimed at optimizing post-PCNL management in pediatric patients.

Conclusion

In this study, we compared the accuracy of eight machine learning algorithms for predicting SIRS after pediatric PCNL and developed a user-friendly web-based prediction platform based on the best-performing LightGBM algorithm, which may offer a novel scientific tool for individualized risk prediction of postoperative SIRS in the pediatric population. Future directions include multicenter prospective validation and clinical guideline development to optimize pediatric post-PCNL management.

Data Sharing Statement

The datasets generated and analyzed during the current study are available from the corresponding author upon reasonable request.

Ethics Approval and Consent to Participate

This study adhered to the principles of the Declaration of Helsinki and was approved by the Medical Ethics Committee of People's Hospital of Xinjiang Uygur Autonomous Region (Approval No: KY2024120147). The requirement for informed consent was waived by the Medical Ethics Committee of People's Hospital of Xinjiang Uygur Autonomous Region, as the study used anonymized clinical data without compromising patient privacy. All data were de-identified and analyzed confidentially following institutional data protection protocols.

Consent for Publication

All authors approved the final manuscript and the submission to this journal.

Funding

There is no funding to report.

Disclosure

The authors report no conflicts of interest in this work.

References

1. Smeulders N, Cho A, Alshaiban A, et al. Shockwaves and the rolling stones: an overview of pediatric stone disease. *Kidney Int Rep*. 2023;8(2):215–228. doi:10.1016/j.ekir.2022.11.017
2. Carmen Tong CM, Ellison JS, Tasian GE. Pediatric stone disease: current trends and future directions. *Urol Clin North Am*. 2023;50(3):465–475. doi:10.1016/j.ucl.2023.04.009
3. Sturgis MR, Becerra AZ, Khusid JA, et al. The monetary costs of pediatric upper urinary tract stone disease: analysis in a contemporary United States cohort. *J Pediatr Urol*. 2022;18(3):311.e1–311.e8. doi:10.1016/j.jpurol.2022.02.019
4. Ingvarsdottir SE, Indridason OS, Palsson R, Edvardsson VO. Stone recurrence among childhood kidney stone formers: results of a nationwide study in Iceland. *Urolithiasis*. 2020;48(5):409–417. doi:10.1007/s00240-020-01179-6
5. Yadav P, Madhavan K, Syal S, Farooq A, Srivastava A, Ansari MS. Technique, complications, and outcomes of pediatric urolithiasis management at a tertiary care hospital: evolving paradigms over the last 15 years. *J Pediatr Urol*. 2019;15(6):665.e1–665.e7. doi:10.1016/j.jpurol.2019.09.011
6. Mishra DK, Bhatt S, Palaniappan S, et al. Mini versus ultra-mini percutaneous nephrolithotomy in a paediatric population. *Asian J Urol*. 2022;9(1):75–80. doi:10.1016/j.ajur.2021.06.002
7. Jones P, Hawary A, Beck R, Somani BK. Role of mini-percutaneous nephrolithotomy in the management of pediatric stone disease: a systematic review of literature. *J Endourol*. 2021;35(5):728–735. doi:10.1089/end.2020.0743
8. Zeng G, Zhu W, Somani B, et al. International Alliance of Urolithiasis (IAU) guidelines on the management of pediatric urolithiasis. *Urolithiasis*. 2024;52(1):124. doi:10.1007/s00240-024-01621-z

9. Kumar N, Yadav P, Kaushik VN, et al. Mini-versus standard percutaneous nephrolithotomy in pediatric population: a randomized controlled trial. *J Pediatr Urol*. 2023;19(6):688–695. doi:10.1016/j.jpurol.2023.08.013
10. Jentzer JC, Lawler PR, van Diepen S, et al. Systemic inflammatory response syndrome is associated with increased mortality across the spectrum of shock severity in cardiac intensive care patients. *Circ Cardiovasc Qual Outcomes*. 2020;13(12):e006956. doi:10.1161/circoutcomes.120.006956
11. Wu W, Zhang D, Jin T, Lu T, Zhou F. Progress in the study of biomarkers for early prediction of systemic inflammatory response syndrome after percutaneous nephrolithotomy. *Front Immunol*. 2023;14:1142346. doi:10.3389/fimmu.2023.1142346
12. Kriplani A, Pandit S, Chawla A, et al. Neutrophil-lymphocyte ratio (NLR), platelet-lymphocyte ratio (PLR) and lymphocyte-monocyte ratio (LMR) in predicting systemic inflammatory response syndrome (SIRS) and sepsis after percutaneous nephrolithotomy (PNL). *Urolithiasis*. 2022;50 (3):341–348. doi:10.1007/s00240-022-01319-0
13. Li P, Tang Y, Zeng Q, et al. Diagnostic performance of machine learning in systemic infection following percutaneous nephrolithotomy and identification of associated risk factors. *Heliyon*. 2024;10(10):e30956. doi:10.1016/j.heliyon.2024.e30956
14. He Y, Xia D, Tong Y, et al. Predictive value of CD3(+) cells and interleukin 2 receptor in systemic inflammatory response syndrome after percutaneous nephrolithotomy. *Front Immunol*. 2022;13:1017219. doi:10.3389/fimmu.2022.1017219
15. Akkas F, Karadag S, Haciislamoglu A. Does the duration between urine culture and percutaneous nephrolithotomy affect the rate of systemic inflammatory response syndrome postoperatively?. *Urolithiasis*. 2021;49(5):451–456. doi:10.1007/s00240-021-01245-7
16. Garriga R, Mas J, Abraha S, et al. Machine learning model to predict mental health crises from electronic health records. *Nat Med*. 2022;28 (6):1240–1248. doi:10.1038/s41591-022-01811-5
17. Brendlin AS, Peisen F, Almansour H, et al. A machine learning model trained on dual-energy CT radiomics significantly improves immunotherapy response prediction for patients with stage IV melanoma. *J Immunother Cancer*. 2021;9(11):e003261. doi:10.1136/jitc-2021-003261
18. An ZY, Wu YJ, Hou Y, et al. A life-threatening bleeding prediction model for immune thrombocytopenia based on personalized machine learning: a nationwide prospective cohort study. *Sci Bull*. 2023;68(18):2106–2114. doi:10.1016/j.scib.2023.08.001
19. Zhang T, Zhu L, Wang X, et al. Machine learning models to predict systemic inflammatory response syndrome after percutaneous nephrolithotomy. *BMC Urol*. 2024;24(1):140. doi:10.1186/s12894-024-01529-1
20. Goldstein B, Giroir B, Randolph A. International pediatric sepsis consensus conference: definitions for sepsis and organ dysfunction in pediatrics. *Pediatr Crit Care Med*. 2005;6(1):2–8. doi:10.1097/01.Pcc.0000149131.72248.E6
21. Mujahid M, Kına E, Rustam F, et al. Data oversampling and imbalanced datasets: an investigation of performance for machine learning and feature engineering. *J Big Data*. 2024;11(1):87. doi:10.1186/s40537-024-00943-4
22. Chen X, Zhang H, Guo D, et al. Risk of intraoperative hemorrhage during cesarean scar ectopic pregnancy surgery: development and validation of an interpretable machine learning prediction model. *EClinicalMedicine*. 2024;78:102969. doi:10.1016/j.eclinm.2024.102969
23. Huang Z, Martin J, Huang Q, Ma J, Pei F, Huang C. Predicting postoperative transfusion in elective total hip and knee arthroplasty: comparison of different machine learning models of a case-control study. *Int J Surg*. 2021;96:106183. doi:10.1016/j.ijsu.2021.106183
24. Guha A, Stabellini N, Shanahan J, et al. ASCVD risk scores versus a novel cancer-specific machine learning-based calculator among patients with breast, colorectal, lung or prostate cancer. *Eur Heart J*. 2024;45(Supplement_1). doi:10.1093/eurheartj/ehae666.3191
25. Zhu L, Jiang R, Pei L, Li X, Kong X, Wang X. Risk factors for the fever after percutaneous nephrolithotomy: a retrospective analysis. *Transl Androl Urol*. 2020;9(3):1262–1269. doi:10.21037/tau.2020.03.37
26. Kaygısız O, Satar N, Güneş A, et al. Factors predicting postoperative febrile urinary tract infection following percutaneous nephrolithotomy in prepubertal children. *J Pediatr Urol*. 2018;14(5):448.e1–448.e7. doi:10.1016/j.jpurol.2018.04.010
27. Puia D, Gheorghincă Ş, Radavoi GD, Jinga V, Pricop C. Can we identify the risk factors for SIRS/sepsis after percutaneous nephrolithotomy? A meta-analysis and literature review. *Exp Ther Med*. 2023;25(3):110. doi:10.3892/etm.2023.11809
28. Walters S, Porter C, Brophy PD. Dialysis and pediatric acute kidney injury: choice of renal support modality. *Pediatr Nephrol*. 2009;24(1):37–48. doi:10.1007/s00467-008-0826-x
29. Ordon M, Andonian S, Blew B, Schuler T, Chew B, Pace KT. CUA guideline: management of ureteral calculi. *Can Urol Assoc J*. 2015;9(11–12): E837–51. doi:10.5489/cuaj.3483
30. Diaz-Ricart M, Torramade-Moix S, Pascual G, et al. Endothelial damage, inflammation and immunity in chronic kidney disease. *Toxins*. 2020;12 (6):361. doi:10.3390/toxins12060361
31. Rashid H, Jali A, Akhter MS, Abdi SAH. Molecular mechanisms of oxidative stress in acute kidney injury: targeting the loci by resveratrol. *Int J Mol Sci*. 2023;25(1):3. doi:10.3390/ijms25010003
32. Malek M, Nematbakhsh M. Renal ischemia/reperfusion injury; from pathophysiology to treatment. *J Renal Injury Prev*. 2015;4(2):20–27. doi:10.12861/jrip.2015.06
33. Quigley R. Diagnosis of urinary tract infections in children. *Curr Opin Pediatr*. 2009;21(2):194–198. doi:10.1097/MOP.0b013e328326f702
34. Rivera M, Viers B, Cockerill P, Agarwal D, Mehta R, Krambeck A. Pre- and postoperative predictors of infection-related complications in patients undergoing percutaneous nephrolithotomy. *J Endourol*. 2016;30(9):982–986. doi:10.1089/end.2016.0191
35. Xu D, Dai R, Chi H, Ge W, Rong J. Long non-coding RNA MEG8 suppresses hypoxia-induced excessive proliferation, migration and inflammation of vascular smooth muscle cells by regulation of the miR-195-5p/RECK axis. *Front Mol Biosci*. 2021;8:697273. doi:10.3389/fmolb.2021.697273
36. Coates CJ, Decker H. Immunological properties of oxygen-transport proteins: hemoglobin, hemocyanin and hemerythrin. *Cell Mol Life Sci*. 2017;74(2):293–317. doi:10.1007/s00018-016-2326-7
37. Amri F, Ghouili I, Tonon MC, Amri M, Masmoudi-Kouki O. Hemoglobin-improved protection in cultured cerebral cortical astroglial cells: inhibition of oxidative stress and caspase activation. *Front Endocrinol*. 2017;8:67. doi:10.3389/fendo.2017.00067
38. Matsumoto H, Yamakawa K, Ogura H, Koh T, Matsumoto N, Shimazu T. Clinical significance of tissue factor and CD13 double-positive microparticles in sirs patients with trauma and severe sepsis. *Shock*. 2017;47(4):409–415. doi:10.1097/shk.0000000000000768
39. Austermann J, Roth J, Barczyk-Kahlert K. The good and the bad: monocytes' and macrophages' diverse functions in inflammation. *Cells*. 2022;11 (12):1979. doi:10.3390/cells11121979